Cone-beam computed tomography with a flat-panel imager:
Magnitude and effects of x-ray scatter

Jeffrey H. Siewerdsena) and David A. Jaffray
Department of Radiation Oncology, William Beaumont Hospital, Royal Oak, Michigan 48073

Speaker: Cyong-Lian Guo(郭瓊蓮)

Outline

➢ **INTRODUCTION**

➢ **METHODS AND MATERIALS**

➢ **RESULTS**

➢ **DISCUSSION AND CONCLUSIONS**

Introduction

➢When?

➢Why?

➢How?

➢What?

When?

➢ P. C. Johns and M. Yaffe, ''Scattered radiation in fan beam imaging systems,'' Med. Phys. **9**, 231–239 (1982)

➢ G. H. Glover, ''Compton scatter effects in CT reconstructions,'' Med. Phys. **9**, 860–867 (1982)

➢ P. M. Joseph and R. D. Spital, ''The effects of scatter in x-ray computed tomography,'' Med. Phys. **9**, 464–472 (1982)

➢ D. A. Jaffray, J. H. Siewerdsen, G. E. Edmundson, J. W. Wong, and A. Martinez, ''Cone-beam CT: Applications in image-guided external beam radiotherapy and brachytherapy,'' Meeting of the World Congress on Medical Physics and Biomedical Engineering, Chicago, IL, July 23–28 (2000) (abstract).

➢ Wojciech Zbijewski, ''Efficient Monte Carlo Based Scatter ArtifactReduction in Cone-Beam Micro-CT'' IEEE Transactions on Medical Imaging,vol.25,No.7,JULY 2006

Why?

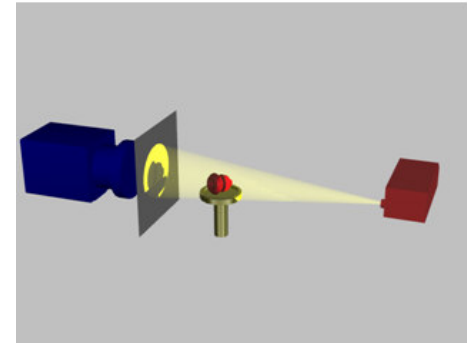- ➤ CBCT(cone-beam computed tomography)
  - a. FPI
  - b. FDK reconstruction
- ➤ CBCT-scatter
  - a. cup and streak artifact
  - b. CT#
  - c. contrast , noise
- ➤ Solution
  - a. correction algorithm
  - b. grid
  - c. focused collimator
  - d. air gap

How?

➢ Quantify scatter
  – Shading artifacts and CT number inaccuracy
  – Effect of x-ray scatter on contrast
  – Effect of x-ray scatter on voxel noise
  – Effect of x-ray scatter on CNR

What?
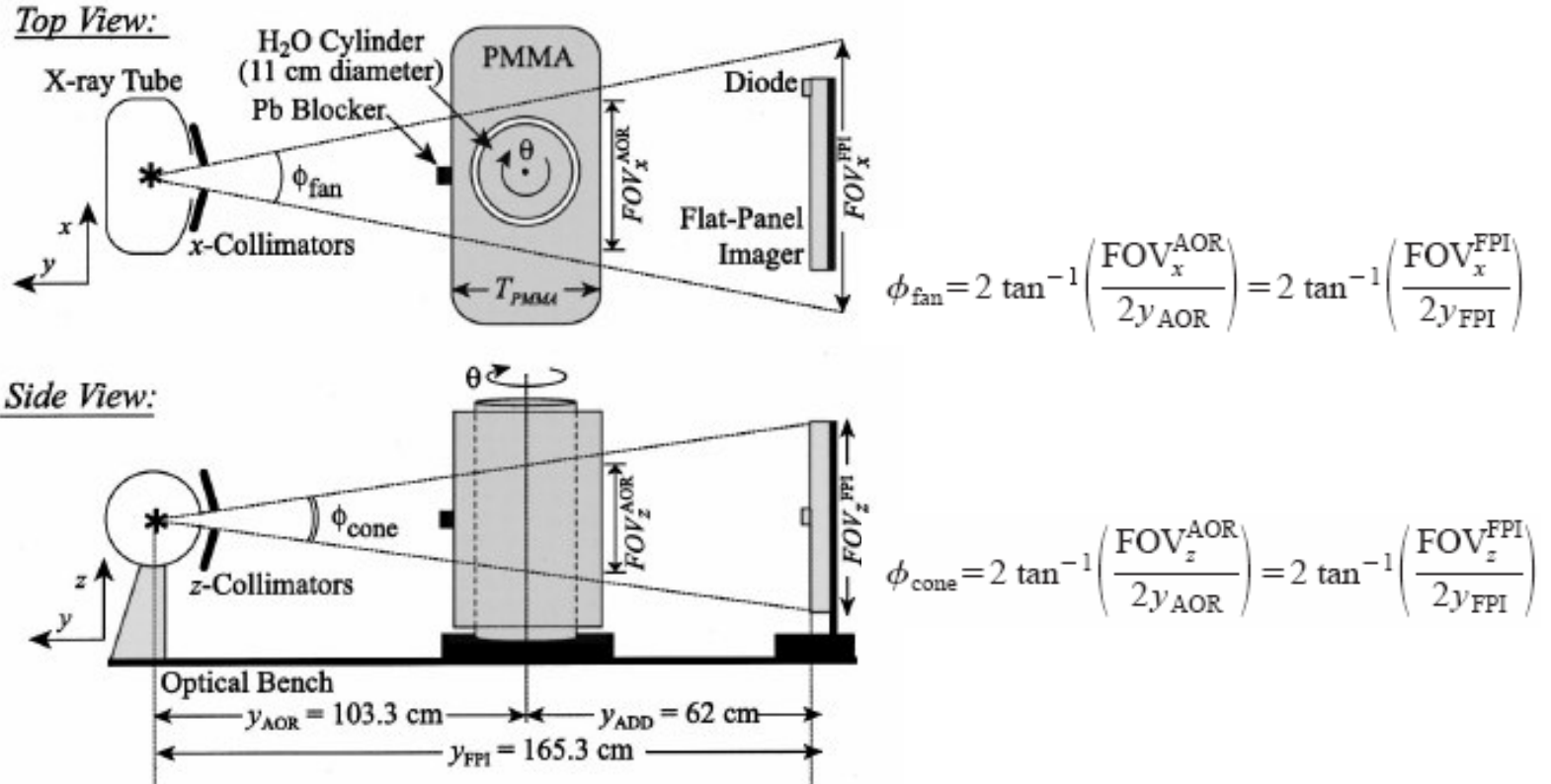
METHODS AND MATERIALS

-experimental setup

FIG. 1. Schematic illustration of the experimental setup used to measure the magnitude and effects of x-ray scatter in flat-panel cone-beam CT. The x-ray tube, rotating object, and FPI operate synchronously to acquire projection data for cone-beam reconstruction. The magnitude of x-ray scatter was varied through adjustment of the fan angle (ϕ_{fan}), the cone angle (ϕ_{cone}), and the thickness of PMMA (T_{PMMA}) surrounding a rotating water-filled cylinder. The Pb blocker was used for measurement of the SPR at the detector plane.
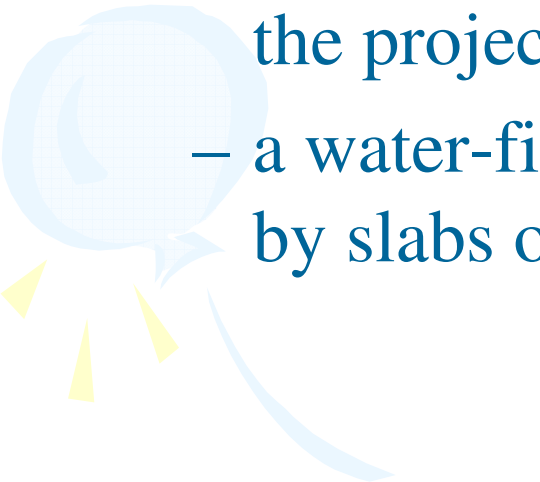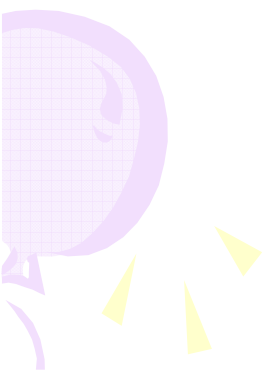
Experimental setup

➢ General Electric (Milwaukee), (WI) Maxiray 75

➢ 120 kVp with 0.5-mm Cu filtration

➢ Exposure was measured using an RTI Electronics (Molndal, Sweden) PMX-III multimeter and is reported either in terms of the exposure in air at isocenter, X_{iso} , or at the center of the FPI, X_{FPI}

Experimental setup

➢Phantom

– FPI-CBCT imaging without lateral truncation of the projection

– a water-filled cylinder (11 cm diameter)surrounded by slabs of polymethyl methacrylate (PMMA).

Experimental setup

➤ The magnitude of x-ray scatter at the detector plane

➤ The range in selected fan angle, cone angle, and object thickness correspond to conditions expected in the clinical setting.

Magnitude of x-ray scatter

➢ The SPR at the detector plane was measured in a manner similar to that of Johns and Yaffe.

➢ A Pb blocker (9-mm-diam disk, 10 mm thick)was placed at the entrance of the phantom on the central axis of the beam. For each measurement of SPR, ten projections were acquired with the FPI, five with the blocker in place and five with the blocker removed.

– Scatter only signal(with blocker)
– Scatter+primary signal(without blocker)

Magnitude of x-ray scatter

- ➢ Measurements of SPR
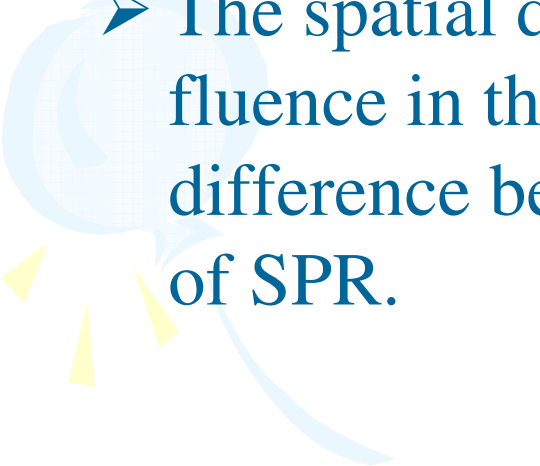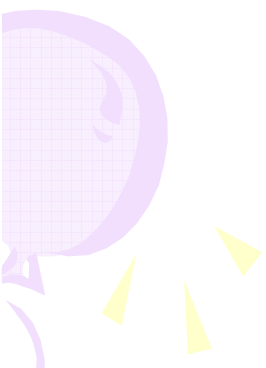 - • were performed using Pb blockers ranging in diameter from 5 to 15mm
- ➢ Human anatomy
  - • PMMA slabs were placed in simple rectangular arrangements approximating the AAPM standard phantoms
- ➢ The SPR was also measured for each configuration of ffan , fcone , and T_{PMMA} used in measurements

Magnitude of x-ray scatter

➢ Spatial distribution of x-ray scatter in the detector plane.(fig1)

➢ The spatial distribution of x-ray scatter energy fluence in the detector plane was computed from the difference between the images acquired as a function of SPR.

Shading artifacts and CT number inaccuracy

➢Two types of shading artifact

– ''cup''

– ''streak.''

$$\Delta = 100 \times \frac{\langle \mu \rangle - \mu_{H_2O}}{\mu_{H_2O}}.$$

To quantify the inaccuracy of voxel values,

$$t_{cup} = 100 \times \frac{\mu_{edge} - \mu_{center}}{\mu_{edge}}.$$

To quantify the degree of spatial nonuniformity, voxel values near the center of the reconstruction, u center , were compared to those at ;5 mm inside the edge of the cylinder, u edge , giving the degree of ''cupping:''
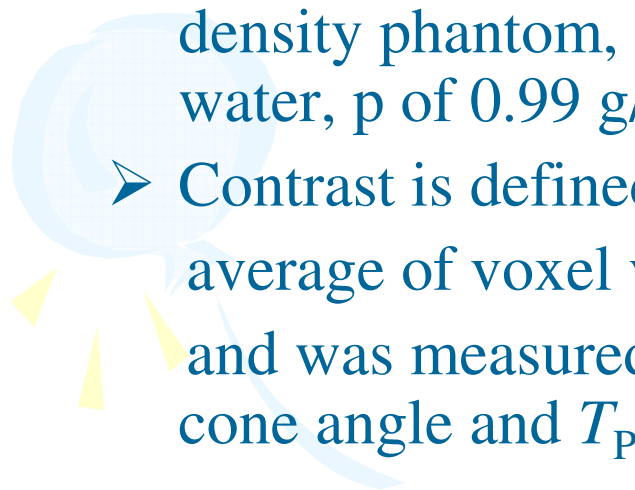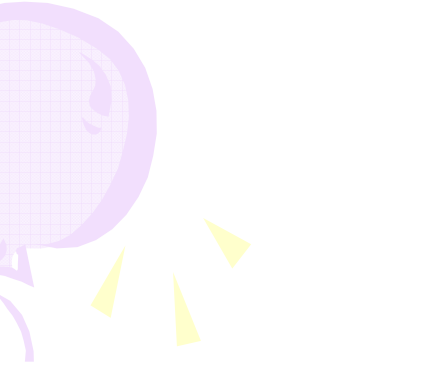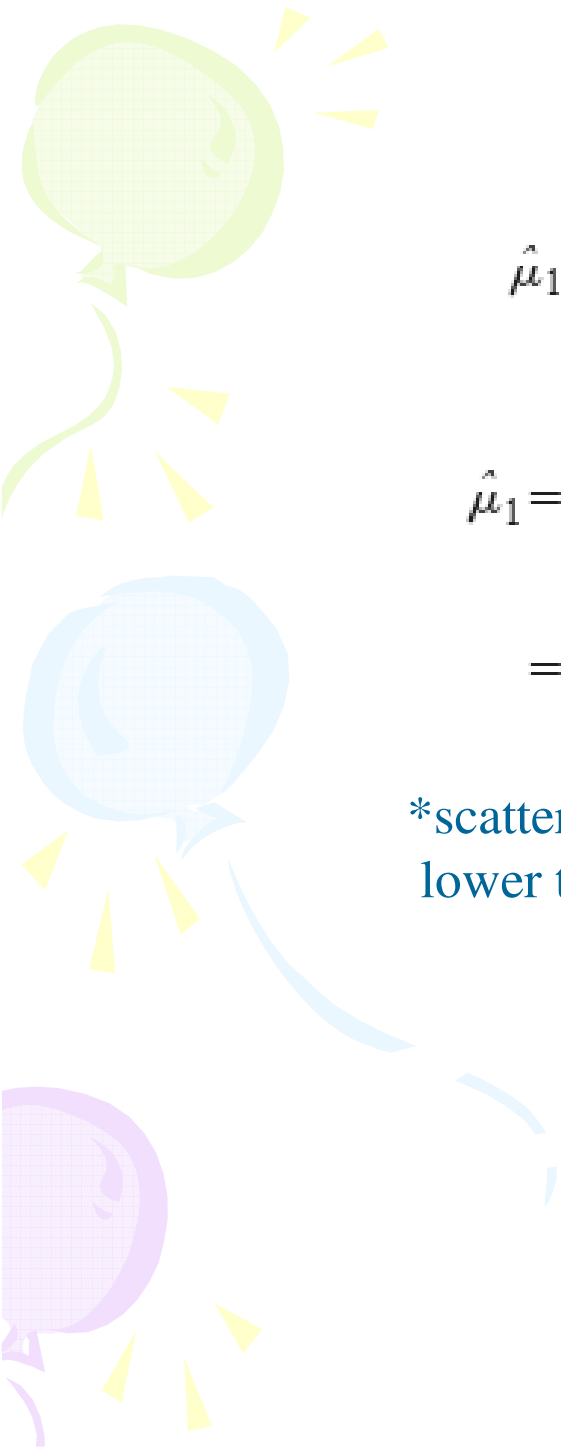
streak artifact

- two 2.8-cm-diam ''bone'' inserts placed within the water cylinder(electron density,1.707 times that of water ; physical density,1.84 g/cm^3, CT#= 1367.8)

- it does provide qualitative visualization of the magnitude of such artifacts as a function of SPR across a range that is representative of that anticipated in the clinical setting.

Effect of x-ray scatter on contrast
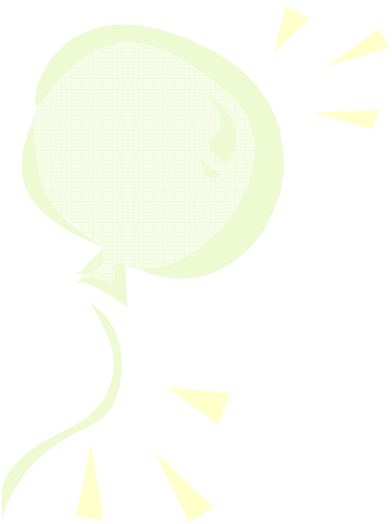
➢ The effect of x-ray scatter on object contrast was investigated using a ''breast-equivalent'' insert placed within the water cylinder (BR SR1 breast from the Gammex RMI electron density phantom, with specified r e , of 0.980 times that of water, p of 0.99 g/cm^3, and approximate CT# of 246.7.)

➢ Contrast is defined as the difference between the ensemble average of voxel values in an insert compared to that in water and was measured as a function of SPR. through variation of cone angle and T_{PMMA}

$$\hat{\mu}_1 d = \ln\left(\frac{P_0}{P}\right) + \ln\left(\frac{1 + S_0/P_0}{1 + S/P}\right)$$

$$\hat{\mu}_1 = \frac{1}{d}\left[\ln\left(\frac{P_0}{P}\right) + \ln\left(\frac{1 + S_0/P_0}{1 + S/P}\right)\right],$$

$$= \mu_1 + \frac{1}{d}\ln\left(\frac{1 + S_0/P_0}{1 + S/P}\right).$$
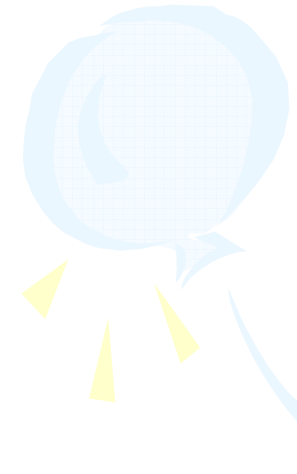
P. C. Johns and M. Yaffe,

*scatter causes voxel values in the reconstruction to be lower than the true attenuation coefficient

$$\hat{\mu}_1 d_1 + \hat{\mu}_2 d_2 = \ln\left(\frac{P_0}{Pe^{\delta\alpha d}}\right) + \ln\left(\frac{1 + S_0/P_0}{1 + S/Pe^{\delta\alpha d}}\right)$$

$$\hat{\mu}_1 (1 - \alpha)d + \hat{\mu}_2 \alpha d = \ln\left(\frac{P_0}{Pe^{\delta\alpha d}}\right) + \ln\left(\frac{1 + S_0/P_0}{1 + S/Pe^{\delta\alpha d}}\right)$$

$$\alpha(\hat{\mu}_1 - \hat{\mu}_2) = \hat{\mu}_1 - \frac{1}{d}\left[\ln\left(\frac{P_0}{Pe^{\delta\alpha d}}\right) + \ln\left(\frac{1 + S_0/P_0}{1 + S/Pe^{\delta\alpha d}}\right)\right]$$

$$\hat{\mu}_1 - \hat{\mu}_2 = \frac{\hat{\mu}_1}{\alpha} - \frac{1}{\alpha d}\left[\ln\left(\frac{P_0}{Pe^{\delta\alpha d}}\right) + \ln\left(\frac{1 + S_0/P_0}{1 + S/Pe^{\delta\alpha d}}\right)\right]$$

$$d_2 = \alpha d \qquad d = d_1 + d_2 \qquad \therefore d_1 = (1 - \alpha)d$$

$$\hat{C} = \hat{\mu}_1 - \hat{\mu}_2,$$

$$= \frac{1}{\alpha d} \left[\ln\left(\frac{P_0}{P}\right) + \ln\left(\frac{1 + S_0/P_0}{1 + S/P}\right) \right] - \frac{1}{\alpha d} \left[\ln\left(\frac{P_0}{Pe^{\delta \alpha d}}\right) \right.$$

$$\left. + \ln\left(\frac{1 + S_0/P_0}{1 + S/Pe^{\delta \alpha d}}\right) \right],$$

$$= \frac{1}{\alpha d} \left[\ln\left(\frac{P_0}{P} \frac{Pe^{\delta \alpha d}}{P_0}\right) + \ln\left(\frac{1 + S_0/P_0}{1 + S/P} \frac{1 + S/Pe^{\delta \alpha d}}{1 + S_0/P_0}\right) \right].$$

$$= \delta + \frac{1}{\alpha d} \ln\left(\frac{1 + S/Pe^{\delta \alpha d}}{1 + S/P}\right).$$

true difference in attenuation coefficients.

increases with SPR degradation in contrast

20

Effect of x-ray scatter on voxel noise

➢ Voxel noise, σ_{vox} , was determined as described previously1 from the average of the standard deviations in circular realizations taken from transaxial slices in water.

$$\frac{\sigma_{\mathrm{vox}}^2}{\mu^2} = \frac{kE_xf_ce^{\mu d/2}I}{\rho\mu h\,\eta D_{\mathrm{center}}\,a_{\mathrm{res}}^3}$$

Barrett, Gordon, and Hershel ''Statistical limitations in transaxial tomography''1976

➢ Voxel noise was measured as a function of SPR by acquiring FPI-CBCT scans of the water cylinderat various settings of fcone , with phantom thickness fixed at T_{PMMA}(30 cm)

Effect of x-ray scatter on CNR

$$C_{AB} = |S_A - S_B|$$

$$CNR_{AB} = \frac{C_{AB}}{\sigma_N} = \frac{|S_A - S_B|}{\sigma_N} = |SNR_A - SNR_B|$$

$$\text{CNR}^2 = \left[\delta + \frac{1}{\alpha d} \ln\left(\frac{1 + S/P e^{\delta \alpha d}}{1 + S/P} \right) \right]^2 \cdot \frac{\rho h \eta D_{\text{center}} \alpha_{\text{res}}^3}{k \mu E_x f_c e^{\mu d/2} I}$$

* CNR can be restored by increasing dose
and/or reducing spatial resolution.

$$\frac{\alpha_{\text{res}}^3 h}{I} D_{\text{center}} = \frac{\text{CNR}^2}{\left[\delta + \frac{1}{\alpha d} \ln\left(\frac{1 + S/P e^{\delta \alpha d}}{1 + S/P} \right) \right]^2} \cdot \frac{k \mu E_x f_c e^{\mu d/2}}{\rho \eta}$$

*analysis the dose and/or spatial resolution required to restore CNR to the value
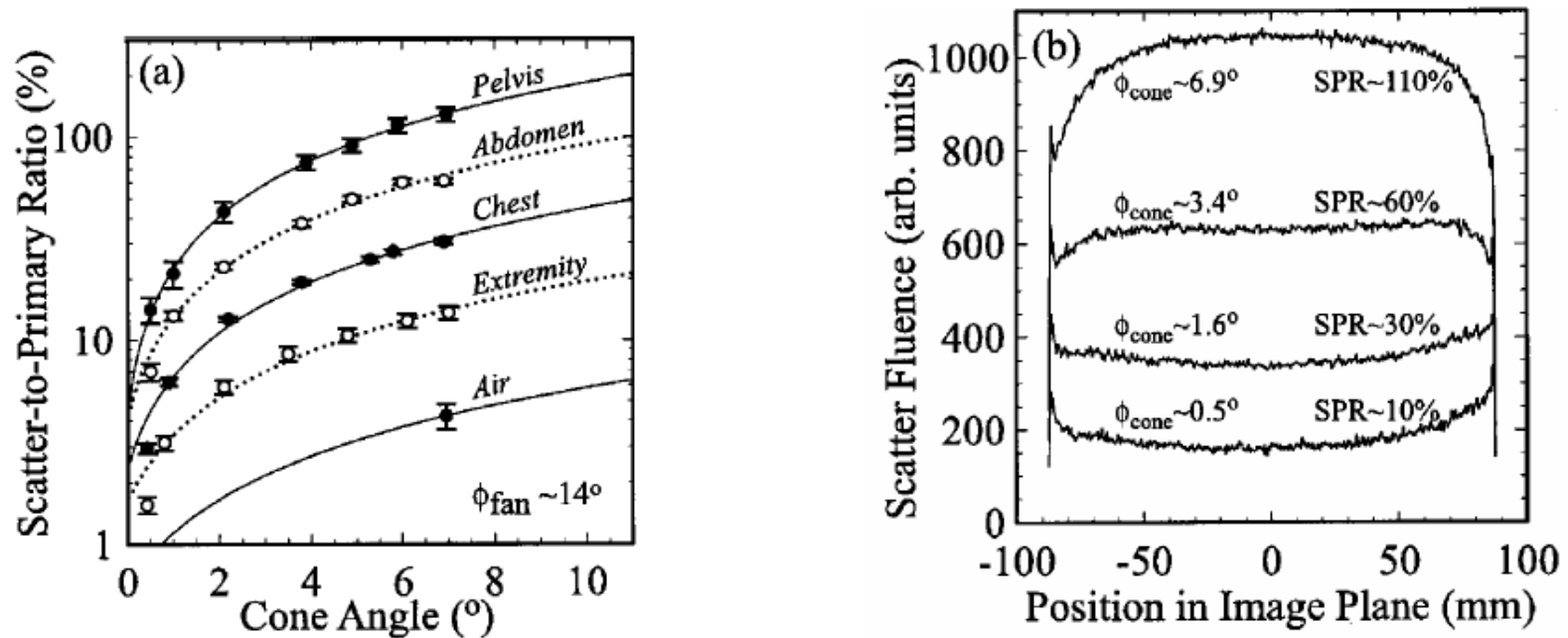
22

Result

FIG. 2. (a) SPR at the detector plane measured as a function of cone angle. The curves are linear fits to the data, showing that the slope (i.e., change in SPR per degree of cone angle) increases for thicker objects. All error bars herein indicate ±1 standard deviation from the mean. (b) Scatter fluence profiles at the detector plane for various settings of cone angle. For small cone angles, the scatter distributions are similar to those in slice-based CT, but increase significantly for larger cone angles.
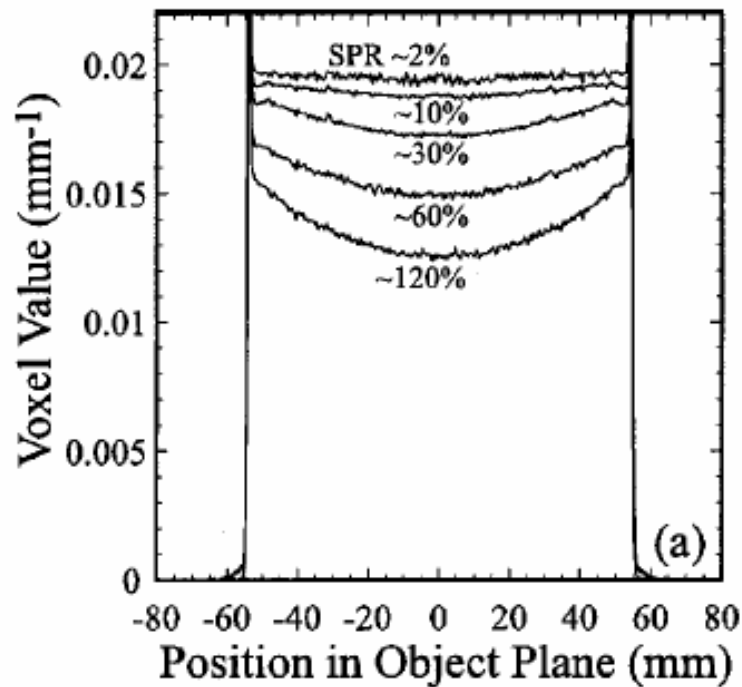
For SPR in excess
of ~100%, average reconstruction values are
 inaccurate (i.e.,underestimated) by more than 30%.

The relative degree of
nonuniformity in the image increases from t_{cup};2% for SPR
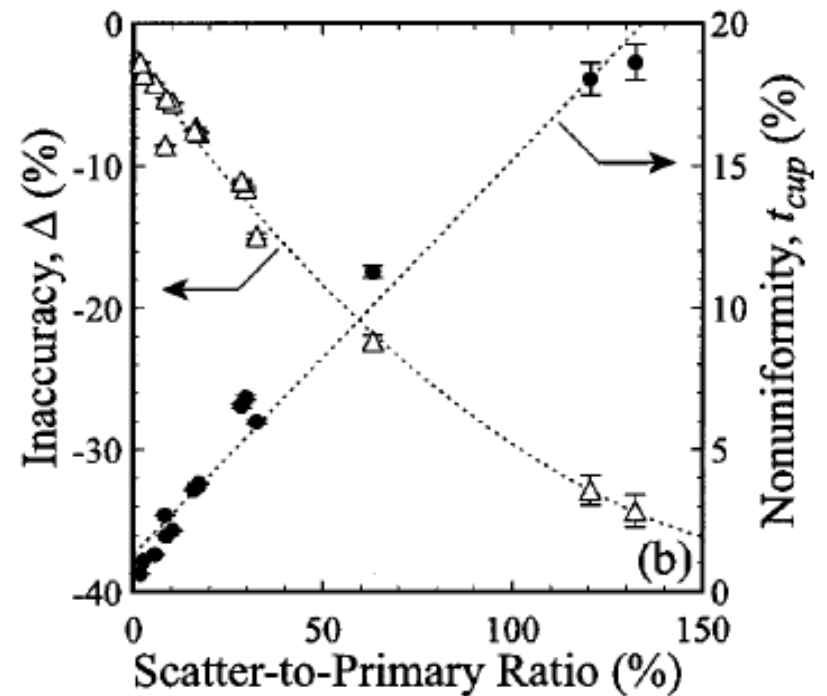(10%) to nearly 20% cupping for SPR in excess of 100%.

FIG. 4. (a) Signal profiles through the center of transverse images of the water phantom, showing the degree of CT# inaccuracy and image nonuniformity at various levels of SPR. The inaccuracy, Δ, defined as the percent deviation in mean reconstruction value from the expected value, is plotted versus SPR on the left-hand axis of (b). The nonuniformity, t_{cup}, defined as the relative deviation between voxel values in the center of the reconstruction compared to those at the edge, is plotted on the right-hand axis of (b).
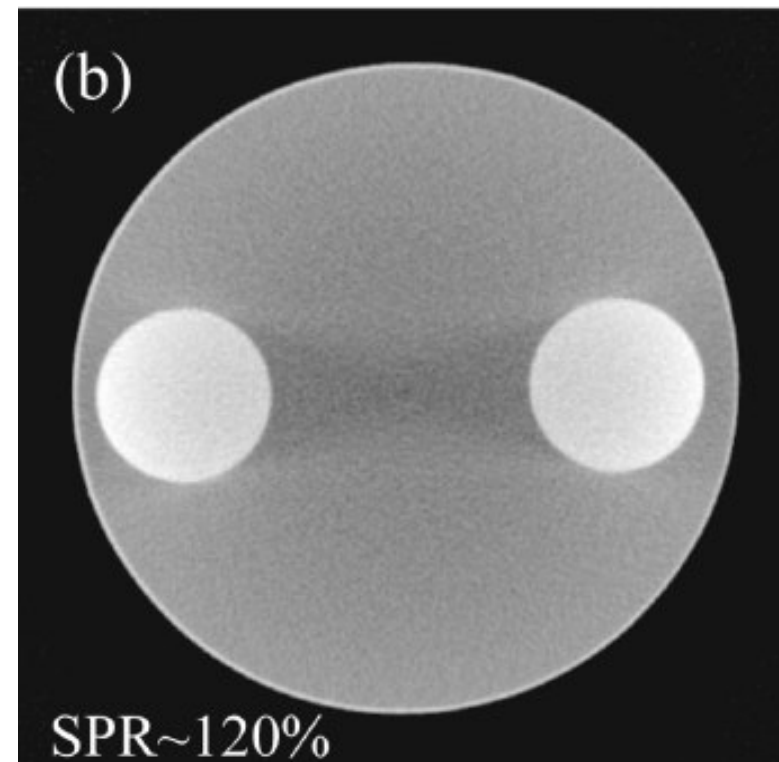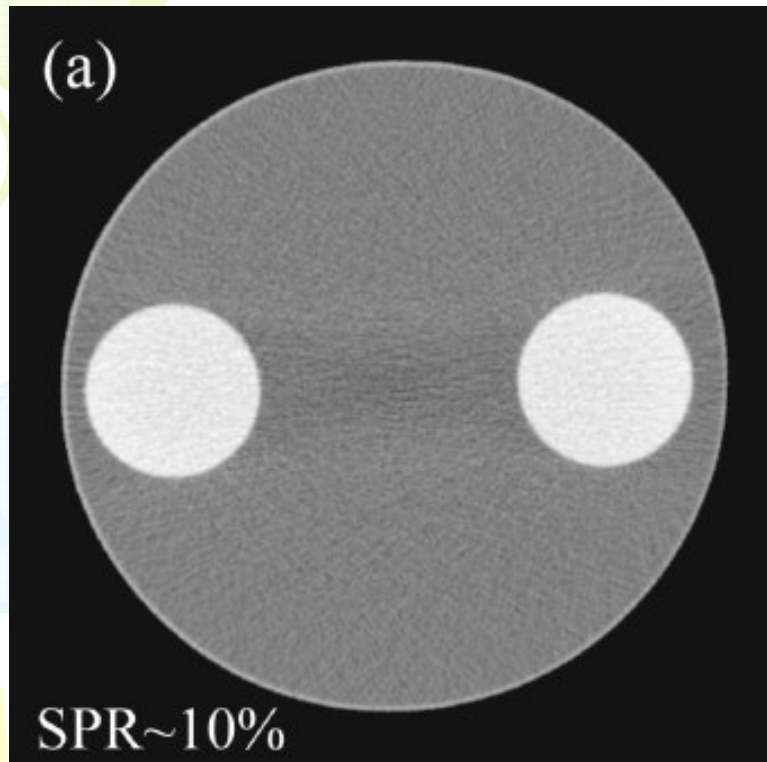
24

FIG. 5. Transaxial images of a water cylinder containing two bone inserts acquired under conditions of (a) low- and (b) high-scatter conditions. The former exhibits faint streak and photon starvation artifacts between the inserts. At higher SPR, the well-known streak artifact becomes prominent. These images and those of Fig. 3 qualitatively illustrate the magnitude of common x-ray scatter artifacts for scatter conditions expected in the clinical setting.
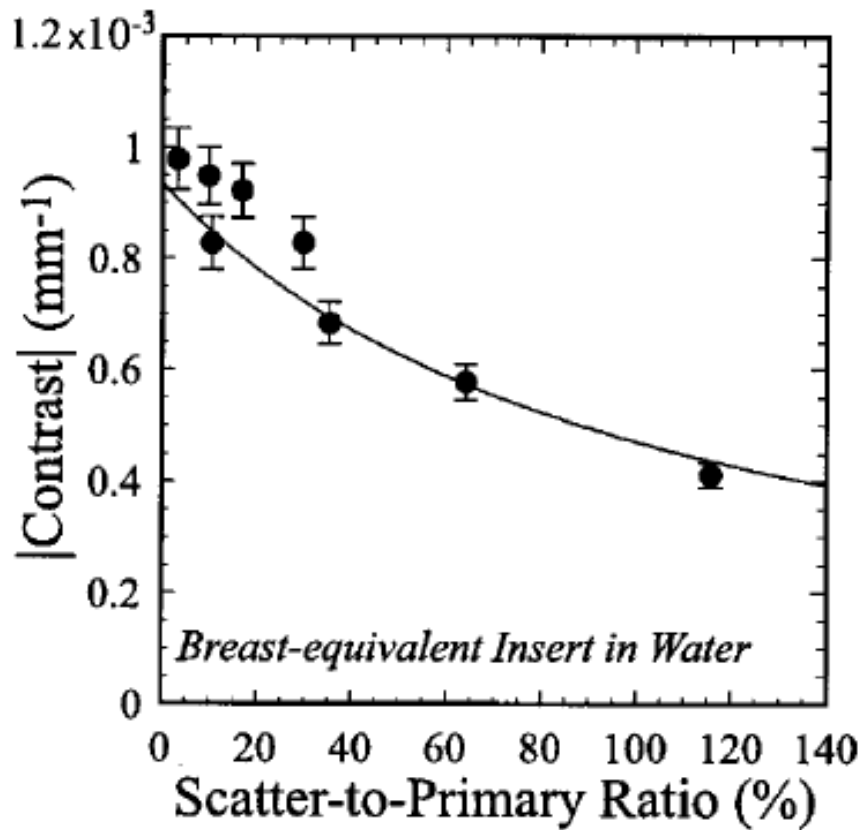
$$\hat{C} = \hat{\mu}_1 - \hat{\mu}_2,$$

$$= \frac{1}{\alpha d}\left[\ln\left(\frac{P_0}{P}\right) + \ln\left(\frac{1+S_0/P_0}{1+S/P}\right)\right] - \frac{1}{\alpha d}\left[\ln\left(\frac{P_0}{Pe^{\delta\alpha d}}\right)\right]$$

$$+ \ln\left(\frac{1+S_0/P_0}{1+S/Pe^{\delta\alpha d}}\right)\Bigg],$$

$$= \frac{1}{\alpha d}\left[\ln\left(\frac{P_0}{P}\frac{Pe^{\delta\alpha d}}{P_0}\right) + \ln\left(\frac{1+S_0/P_0}{1+S/P}\frac{1+S/Pe^{\delta\alpha d}}{1+S_0/P_0}\right)\right]$$

$$= \delta + \frac{1}{\alpha d}\ln\left(\frac{1+S/Pe^{\delta\alpha d}}{1+S/P}\right).$$

FIG. 6. Effect of x-ray scatter on FPI-CBCT contrast. The contrast between a breast-equivalent insert and water decreases from ~ 0.0009 mm^{-1} (i.e., $\sim 5\%$ relative contrast) at low scatter conditions to ~ 0.0004 mm^{-1} (i.e., $\sim 2.2\%$ relative contrast) at SPR $\sim 100\%$. The effect is described well by the simple analytical form of Eq. (3d).

Discussion & Conclution

➢ The analogy to projection imaging is obvious: just as 2D projection imagers must contend with higher levels of scatter than 1D linear scanning detectors, so must 3D volumetric imagers (e.g., FPI-CBCT) contend with higherlevels than conventional tomographic imagers (e.g., slice based CT)

➢ The effect of x-ray scatter on the contrast, noise, and contrast-to-noise ratio (CNR) in FPI-CBCT reconstructions was measured as a function of SPR and compared to predictions of a simple analytical model.

➢ The benefits of volumetric imaging, however,warrant investigation of how best to reduce x-ray scatter and manage its deleterious effects.

Reference

➢ D. A. Jaffray and J. H. Siewerdsen, ''Cone-beam computed tomography with a flat-panel imager: Initial performance characterization,'' Med. Phys. **27**, 1311–1323 (2000).

➢ G. H. Glover, ''Compton scatter effects in CT reconstructions,'' Med. Phys. **9**, 860–867 (1982)

➢ P. M. Joseph and R. D. Spital, ''The effects of scatter in x-ray computed tomography,'' Med. Phys. **9**, 464–472 (1982)

➢ D. A. Jaffray, J. H. Siewerdsen, G. E. Edmundson, J. W. Wong, and A. Martinez, ''Cone-beam CT: Applications in image-guided external beam radiotherapy and brachytherapy,'' Meeting of the World Congress on Medical Physics and Biomedical Engineering, Chicago, IL, July 23–28 (2000) (abstract).

➢ Wojciech Zbijewski, ''Efficient Monte Carlo Based Scatter ArtifactReduction in Cone-Beam Micro-CT'' IEEE Transactions on Medical Imaging,vol.25,No.7,JULY 2006